Glow-discharge sheath electric fields: Negative-ion, power, and frequency effects

Richard A. Gottscho
AT&T Bell Laboratories, Murray Hill, New Jersey 07974-2070
(Received 2 February 1987)

Using Stark-mixed laser-induced fluorescence, space-time–resolved maps of sheath electric fields in discharges through BCl_3 and Ar are measured as a function of concentration, power density (0.14–0.41 $W\,cm^{-3}$), and frequency (dc to 10 MHz). Sheath oscillations are observed throughout this frequency range and are discussed qualitatively in terms of characteristic times for ion and electron transport. Double layers are observed in low-frequency discharges containing more than 5% BCl_3 and are attributed to a buildup in negative-ion concentration; it is argued that different ratios of negative-ion to electron density in the plasma and sheath are responsible for double-layer formation at the plasma-sheath boundary. These maps should prove useful as input for particle transport simulations in plasma-processing and light-source applications. They also provide stringent tests for self-consistent sheath theories.

I. INTRODUCTION

For applications of plasmas to materials processing, e.g., thin-film etching and deposition, the sheath, or boundary layer between the plasma and the surface, is of paramount importance. Ion and electron modification of deposition rates, etching rates, and electronic properties is a function of the charged-particle energy and flux,[1,2] which are governed by the shape and magnitude of the sheath electric field.[3,4] For example, if the field E is uniform throughout the sheath and the collisional mean free path λ is small compared with the sheath thickness, charged particles will impact the surface with an energy λE. On the other hand, if the field is large for only a small distance (for example, if a double layer exists[5–7]) at the plasma-sheath boundary, charged particles will impact the surface with only thermal energies. Clearly, for reliable simulations of charged-particle transport to surfaces, it is necessary to know the shapes and magnitudes of the sheath fields. Measurements of sheath electric fields are also central to the study of discharge nonlinearities,[8] the testing of self-consistent discharge models,[9–15] and the validity of non-self-consistent models that require sheath fields as input.[16–19]

The sheath electric field is measured for discharges through BCl_3 and mixtures of BCl_3 and Ar over a range of frequencies from dc to 10 MHz. Discharges containing BCl_3 are chosen for study because they are used in plasma etching of Si, Al, and III-V materials.[20–24] They also provide a convenient source of BCl molecules whose Stark-mixed laser-induced fluorescence spectrum can be used to determine the magnitude of the sheath electric field with high spatial and temporal resolution.[25,26] Similar techniques for measuring plasma electric fields have been reported recently.[27–31]

The primary questions that we address here are the following: (1) What changes occur in the sheath as a result of negative-ion formation (Secs III A and III B), (2) how do sheath fields depend on power density (Sec. III B), and (3) how do sheath fields depend on operating frequency (Sec. III C)? These questions are important from both technological and scientific perspectives. Technologically, plasma processes often work by mixing electronegative (Cl_2, BCl_3, O_2, etc.) and electropositive gases (He, Ar, N_2, etc.). However, the negative-ion to electron density ratio, which influences the shape and magnitude of the sheath fields, depends on the feedstock composition;[32–37] thus, mixing electronegative and electropositive gases changes more than just the plasma chemistry. From a scientific perspective, the mechanisms by which power is dissipated and the plasma is sustained are not entirely clear for radio-frequency discharges. In particular, the effects of negative-ion formation, oscillatory plasma-sheath boundaries, and operating frequency on power dissipation and discharge sustenance are not well characterized. As illustrated recently,[38–50] frequency can be an important parameter for controlling discharge kinetics and power dissipation. Frequency-dependent oscillations of the plasma-sheath boundary have been shown theoretically to be an important means by which power is dissipated in rf discharges.[8,51–53] Thus a study of sheath fields as a function of power, frequency, and electronegative gas composition addresses some of the most basic aspects of discharge physics.

II. EXPERIMENTAL PROCEDURE

The discharge is maintained between two equal-area stainless steel electrodes (7.5 cm diameter) spaced 1.6 cm apart. The rf voltage is applied through a matching network, consisting of a transformer for frequencies below 1 MHz and a resonant π circuit for frequencies above 1 MHz. For dc discharges, a 1-kΩ ballast resistor is used in series with the high voltage. The discharge current is measured with a precision of $\sim$10% using a Pearson 4100 transformer in the rf experiments and a Keithley digital multimeter in the dc experiments. Voltage is measured to within 10% using a Tektronix P6015 probe. Power is determined by multiplying instantaneous voltage and current waveforms, acquired using a Tektronix 7854

digital oscilloscope, point-by-point, and then averaging over a single cycle. Voltage and current waveforms are shown in Fig. 1 as a function of concentration, power, and frequency. From experiments in Cl_2 plasmas under similar conditions,[38,54] we estimate the total charge density in the plasma center to be $\sim 10^{11}$ cm^{-3}.

All the experiments described here have been carried out at a pressure of 0.3 Torr and a flow rate of 10 sccm (1 sccm $\equiv$ 1 std. cm^3 min^{-1} $= 4.2 \times 10^{-4}$ mole min^{-1}) with BCl_3 as supplied by Matheson[55,56] and Ar as supplied by Air Products (research grade). Pressure and flow rates are precise to 2% and 10%, respectively; however, the accuracy of these measurements is estimated to be only 5% and 20%, respectively. Although measurements at other pressures (0.1–1.0 Torr) and flow rates (5–30 sccm) have been made, the results are qualitatively similar and are not discussed here.

The laser apparatus has been described in detail previously.[54,57] Briefly, a nitrogen laser is used to pump a tunable dye laser that is then frequency doubled and used to excite the BCl molecule at 272 nm. The laser is fired synchronously with the applied field and the laser and fluorescence collection optics are scanned together so that the dependence of the sheath field on the applied voltage can be measured at any position. Depending on the magnitude of the electric field, either the $P(6)$ or the $P(12)$ rotational transition in the (0,0) vibrational band of the $A\,^1\Pi$-$X\,^1\Sigma^+$ system is pumped.[26] Fluorescence is collected at right angles to the laser beam and spectrally resolved to determine separately the intensities of nominally allowed and forbidden transitions. The ratio of these line intensities is used to determine the magnitude of the sheath electric field. The sign of the electric field cannot be determined from Stark-mixing measurements but is determined for the pure BCl_3 discharges by photodetachment optogalvanic spectroscopy.[58] Fields are measured with spatial and temporal resolutions of 100–200 μm and 10–20 ns, respectively, and a sensitivity of $\sim$75 V/cm.

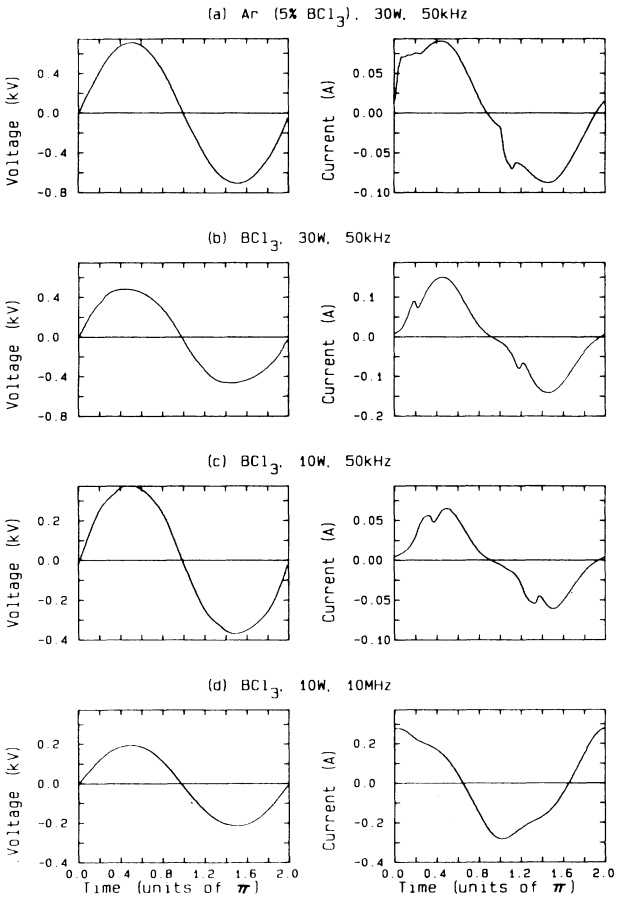

FIG. 1. Voltage (left) and current (right) waveforms at a total pressure of 0.3 Torr and flow rate of 10 sccm for (a) Ar (5% BCl_3), 30 W, 50 kHz; (b) BCl_3, 30 W , 50 kHz; (c) BCl_3, 10 W, 50 kHz; (d) BCl_3, 10 W, 10 MHz.

III. RESULTS AND DISCUSSION

In this section spatially and temporally resolved sheath fields are first examined for discharges through Ar (5% BCl_3) at 50 kHz. The instantaneous response of positive ions and electrons to this low-frequency field governs what is seen in this system; in particular, there are no obvious effects which can be attributed to negative ions. In this sense, this dilute mixture of Ar and BCl_3 is operationally defined to be an electropositive discharge. (Preliminary results from a fluid model of this system suggest that the negative-ion density may be as much as 10 times the electron density in the plasma center.)

Next, by looking at BCl_3 discharges at the same frequency, the effects that negative ions have on the sheath field dynamics and how these effects depend on power density are considered. In the last part of this section, comparisons are made between dc, 50-kHz, and 10-MHz discharges through BCl_3.

A. Sheath dynamics in low-frequency "electropositive" discharges

The sheath electric fields for a 30-W, 50-kHz discharge through Ar (5% BCl_3) are displayed as a space-time, color contour diagram in Fig. 2(a).[59,60] The contour plot is made by linearly interpolating field measurements made at 32 positions in the sheath at 20 times during the rf cycle. Some raw data, field magnitude versus position at a specific time, are shown for the first ($\omega t = \pi$ to 1.5π) and second ($\omega t = 1.5\pi$ to 2π) quarters of the cathodic half cycle in Figs. 3(a) and 4(a), respectively. These profiles are obtained at 1-μsec ($\frac{1}{20}$ cycle at 50 kHz) intervals as shown schematically on the right (time increases from bottom to top).

Sheath expansion is evident from examination of Figs. 2(a) and 3(a); the position of the plasma-sheath boundary moves away from the electrode, as the applied voltage grows more negative. The flat shape of the field near the electrode shows that the space charge density is too small for significant distortion of the applied field. From Poisson's equation,

$$\epsilon_0 \frac{dE}{dx} = e(n_+ - n_e - n_-) , \tag{1}$$

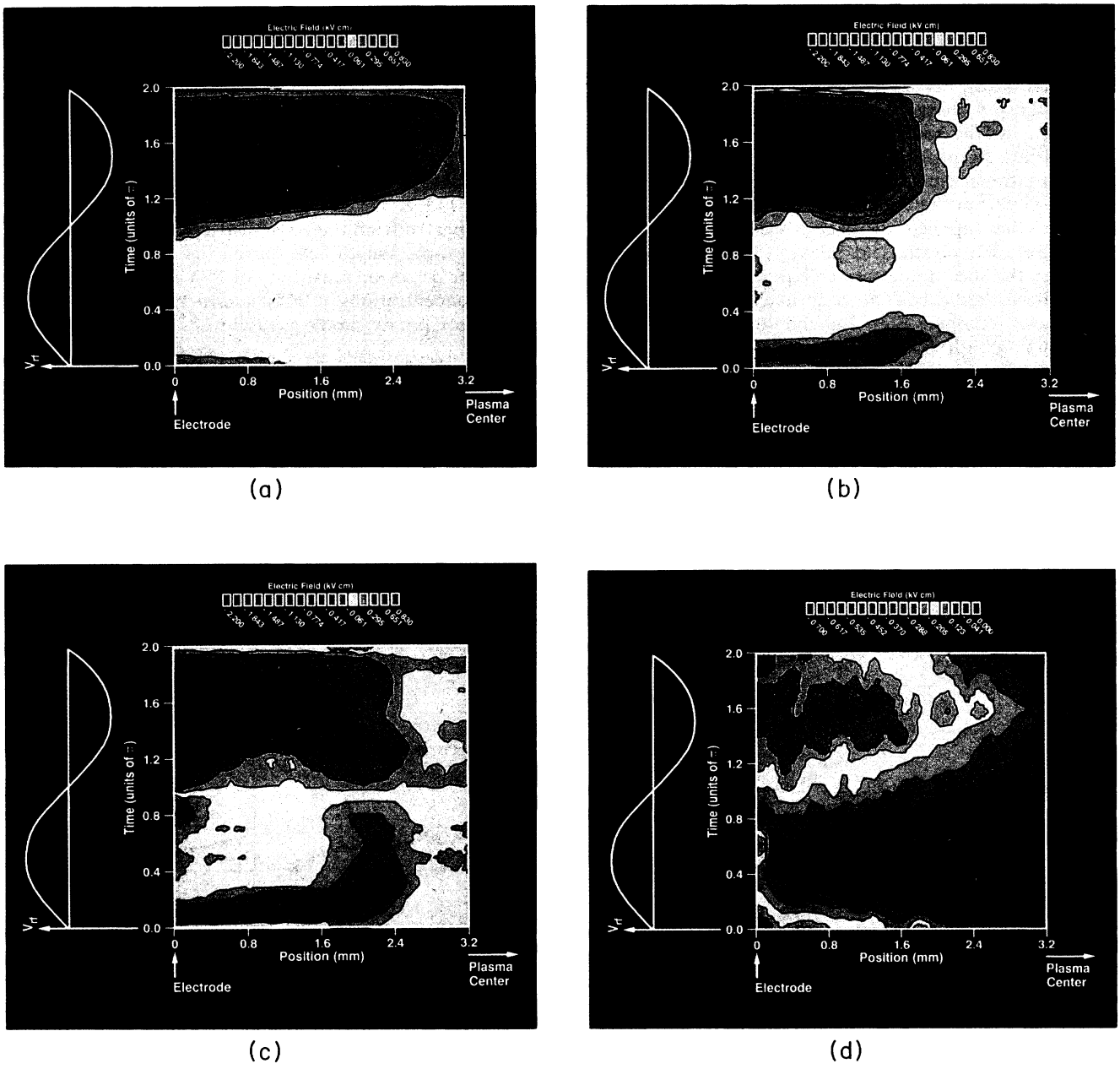

FIG. 2. (a) Color contour plot of sheath electric fields in 50-kHz discharge through 95 at. % Ar and 5 at. % BCl_3. The position of the electrode is at 0 mm and the plasma center (not shown) is at 8.0 mm. Time in units of π refers to the phase of the applied voltage on the electrode at 0 mm as shown by the sine wave on the left. The color scale is shown at the top; the sign of the field is assumed to be positive from $\omega t = 0$ to π and negative from $\omega t = \pi$ to 2π. The plot is generated by linearly interpolating measurements made at 20 equally spaced times during the rf cycle and 32 equally spaced positions in the sheath to a 100×100 space-time array. References 59 and 60 contain additional details on the generation of such plots. Discharge conditions are (see text for measurement precision and accuracy): total flow rate 10 sccm, Ar flow rate 9.5 sccm, BCl_3 flow rate 0.5 sccm, rms voltage 508 V, peak voltage 711 V, rms current 0.064 A, peak current 0.090 A, power 30 W, power density 0.41 W cm^{-3}, pressure 0.3 Torr. (b) Same as (a) except for nominally pure BCl_3 (see Ref. 56). Discharge conditions are the same as for (a) except rms voltage is 354 V, peak voltage is 476 V, rms current is 0.090 A, peak current is 0.146 A. (c) Same as (a) except for nominally pure BCl_3 (see Ref. 56) 10-W, 50-kHz discharge. The sign of the electric field was determined from photodetachment optogalvanic measurements (see Ref. 58). Discharge conditions are the same as for (a) except rms voltage is 274 V, peak voltage is 380 V, rms current is 0.038 A, peak current is 0.065 A, and power density is 0.14 W cm^{-3}. (d) Same as (a) except for nominally pure BCl_3 (see Ref. 56) 10-W, 10-MHz discharge. Discharge conditions are same as for (a) except rms voltage is 147 V, peak voltage is 204 V, rms current is 0.191 A, peak current is 0.281 A, and power density is 0.14 W cm^{-3}. Here, the 100×100 interpolated array is constructed from measurements made at 10 equally spaced times in the rf cycle and 32 equally spaced positions in the rf sheath.

where E is the electric field, n_+ is the positive-ion density, n_e is the electron density, and n_- is the negative-ion density, a flat field ($dE/dx \sim 0$) means that the net charge density is zero. Given the large fields in the cathode sheath, the net charge is small because n_+, n_e, and n_- are small. As the applied field grows more negative, positive ions are swept from the sheath, electrons are repelled back into the plasma, and the plasma-sheath boundary moves away from the electrode surface.[54]

After the applied voltage reaches a minimum ($\omega t = 1.5\pi$), the sheath field relaxes [Figs. 2(a) and 4(a)]. However, the sheath does not collapse in the second quarter of the cathodic half cycle as it expanded during the first quarter [compare Figs. 3(a) and 4(a)]. The position of the plasma-sheath boundary remains unchanged as the field decreases in magnitude from $\omega t = 1.5$ to 2π. The flat shape of the field throughout the sheath [Fig. 4(a)] indicates continued depletion of charge. The asymmetry between sheath expansion and collapse implies that the rate of charge replenishment is slow compared to a quarter cycle. Even though ion-electron pairs may be created by ion-impact and electron-impact processes,[54,61–63] rapid removal by the strong field precludes buildup of space charge. Similarly, diffusion of charge from the plasma into the sheath is slow compared with sheath field extraction at 50 kHz.

As expected from the large disparity in electron and ion mobilities, the sheath field during the anodic half cycle is below the detection sensitivity of 75 V/cm [Fig. (2a)]. For larger concentrations of BCl_3, and therefore n_-, the anodic fields are not negligible as discussed in the following section.

B. Sheath dynamics in low-frequency electronegative discharges

A space-time contour plot of the sheath fields in a 30-W, 50-kHz discharge through BCl_3 is shown in Fig. 2(b). Fields for the first and second quarters of the cathodic half cycle are also shown in Figs. 3(b) and 4(b), respective-

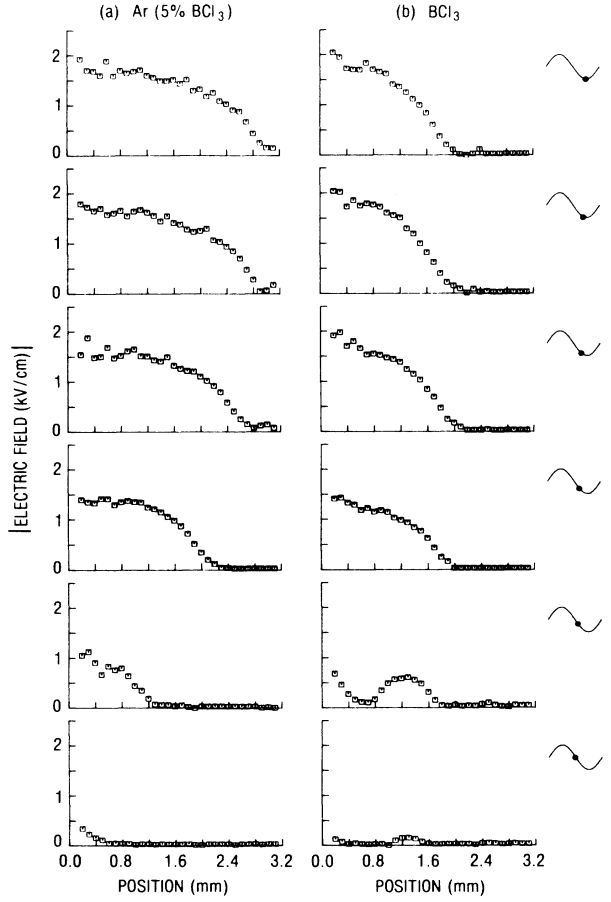

FIG. 3. Sheath electric field magnitudes for first quarter of cathodic half cycle ($\omega t = \pi$ to 1.5π) of 30-W, 50-kHz discharges through (a) Ar (5% BCl_3) and (b) BCl_3 as a function of space and time. Note the expansion of the sheath for the Ar (5% BCl_3) discharge and the formation of double layers for the BCl_3 discharge. See captions to Figs. 1 and 2 for additional discharge conditions.

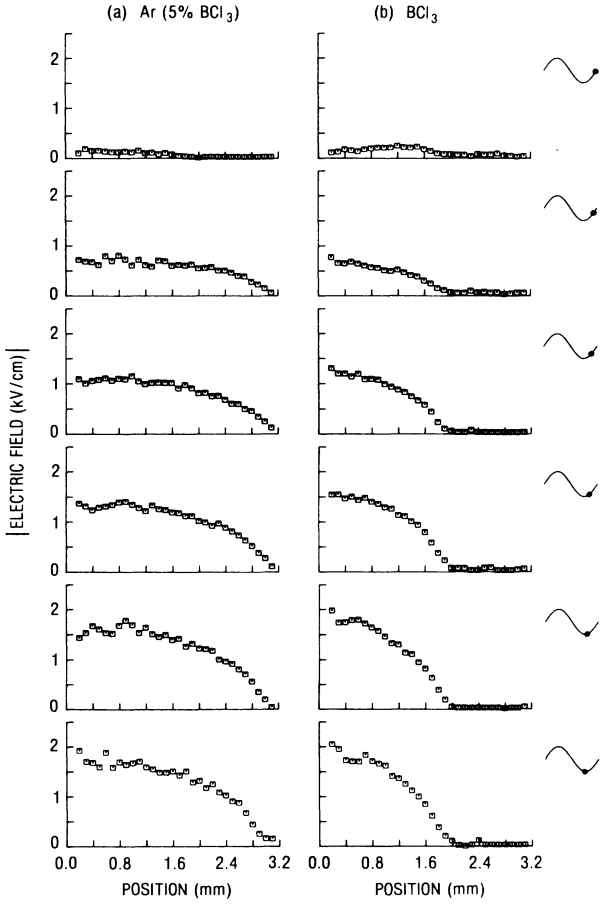

FIG. 4. Same as Fig. 3 except for second quarter of cathodic half cycle ($\omega t = 1.5\pi$ to 2π).

ly. Unlike the electropositive discharge, layers of positive and negative charge density (double layers) are evident from the nonmonotonic variation in the field with position [see Eq. (1)] during the first quarter of the cathodic half cycle. Near the electrode surface, the sheath appears to expand initially, as in the electropositive discharge [compare Figs. 3(a) and 3(b)], but as the applied voltage grows more negative ($\omega t = 0.2\pi$) the expanding sheath merges with the double layer at the plasma-sheath boundary. During the second quarter, the sheath field relaxes in the same manner as in the electropositive case [compare Figs. 4(a) and 4(b)].

The spatial dependence of the sheath field during the first quarter ($\omega t = 0$ to 0.5π) of the anodic half cycle is shown in Fig. 5(a) for a 30-W discharge and Fig. 5(b) for a 10-W discharge. Regardless of power, a large and nearly uniform field is observed at the beginning of the anodic cycle. From photodetachment measurements, the field is found to point toward the plasma, the anode potential lies above the plasma potential, and negative particles are accelerated toward the anode.[58]

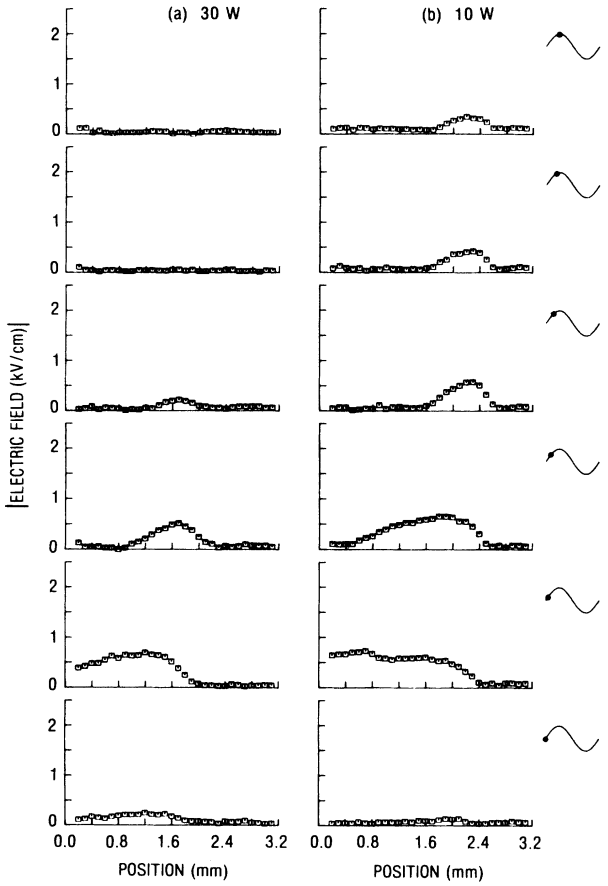

FIG. 5. Sheath electric fields for first quarter of anodic half cycle ($\omega t = 0$ to π) of (a) 30 W and (b) 10-W, 50-kHz discharges through BCl_3 as a function of space and time. Note the large fields at the beginning of the anodic half cycle and the double layers that form subsequently. See caption to Fig. 2 for additional discharge conditions.

1. *Double layers*

Double layers are generally produced in the laboratory by maintaining two adjacent plasmas at different average energies (or temperatures in a Maxwellian system). For example, consider the constricted positive column shown in Fig. 6(a).[6] Although current is continuous across the constriction, the current density is higher in the narrow bore; thus, the electron temperature will be higher in the narrow bore and a potential step forms in order to control transport between the two regions. Since the plasma on each side of the constriction is nearly field-free, each side is nearly an equipotential, and the field at the constriction exhibits a maximum. A simple rationale for the existence of the double layer comes from self-consistency arguments: If two plasmas are adjacent but not at equal temperatures, a potential step must form to convert cold particles into hot particles and *vice versa*. Electrons entering

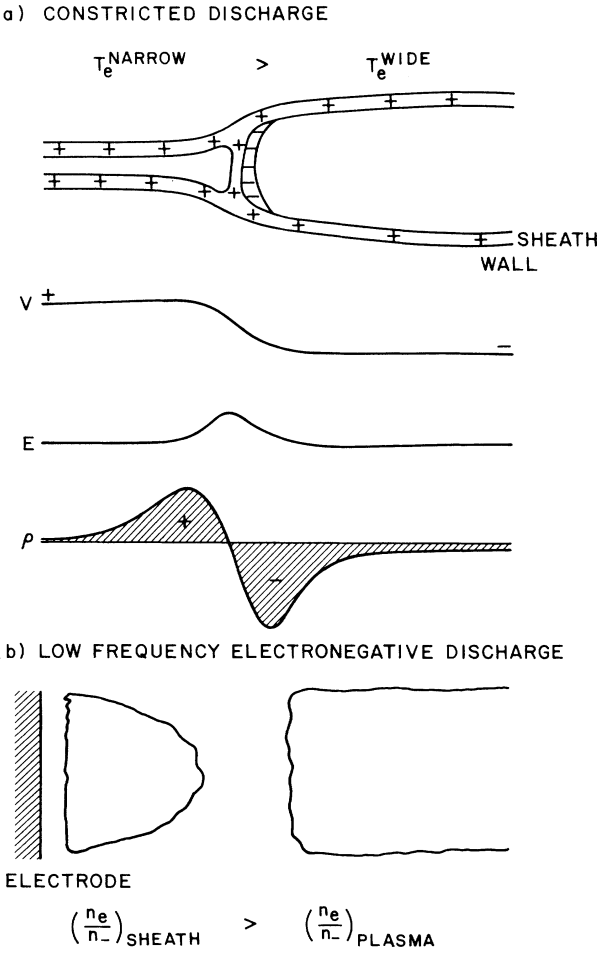

FIG. 6. Schematic illustration after Ref. 6 illustrating analogy between double layers that form in a constricted dc positive column and those that form in a low-frequency electronegative sheath. In both cases, two zones with different negative-particle random energies are maintained by a potential difference at the boundary.

the cold plasma and positive ions entering the hot plasma are slowed, and classically, the density for each type of particle is largest at the turning points on the potential.

In the low-frequency electronegative plasma, double-layer formation suggests that two regions of different average energy exist. But what is the mechanism by which this difference in energy is maintained? Since the double layers are observed only in discharges containing large concentrations of BCl_3, it is likely that negative ions play a significant role. One way in which the average energy can vary in an electronegative discharge is if the electron to negative-ion density ratio changes: The negative-ion temperature, as well as the positive-ion temperature, is close to the bulk gas and wall temperatures in low-pressure glow discharges, but the electron temperature is much higher.

There are at least two reasons why the electron to negative-ion density ratio will vary from plasma to sheath: (1) Negative-ion formation by attachment and loss by detachment is energy and, therefore, field dependent, and (2) electron diffusion and mobility are orders of magnitude larger than ion diffusion and mobility. In the first case, the density ratio will change simply because the balance between formation and loss processes changes from the plasma to the sheath.[64,65] At 50 kHz, electrons lose energy via inelastic collisions with BCl_x molecules at a rate which is fast compared to an rf period. As a result, the attachment rate k_a of electrons to BCl_3, which is rapid for low-energy electrons,[66] is enhanced during the low-voltage, low-field portions of the cycle. Near the zero crossings of the applied voltage waveform ($\omega t = 0$, π, and 2π), relaxation of the electron-energy distribution function (EEDF) can lead to enhanced attachment, formation of an ion-ion plasma, and large fields in both anode and cathode sheaths [Figs. 2(b) and 5]. On the other hand, the negative-ion collisional detachment rate k_d is slow *unless* the ions are accelerated to high energies (~ 20 eV).[67] Thus, negative ions are destroyed easily in the sheath when the sheath fields are large but not so easily in the plasma where the fields are small.

The large anodic fields lead to negative-ion destruction not only by collisional detachment but also by field extraction. Electrons are also swept from the sheath by the strong fields but, unlike the negative and positive ions, they can diffuse from the plasma into the sheath fast enough to partially replenish what is lost by conduction.[68] The electron density will increase relative to the negative-ion density and the ratio of electron to negative-ion density in the sheath will be higher than in the plasma. Recent calculations[68] suggest that double layers form in electronegative plasmas in the absence of collisional detachment and that the differences in ion and electron diffusivity and mobility are primarily responsible for double-layer formation.

Apparently, two conditions must be met for double layers to form in electronegative discharges. First, the negative-ion density must be sufficiently large that negative ions carry a significant portion of the negative current:

$$n_- \gtrsim \frac{n_e \mu_e}{\mu_-} \ . \tag{2}$$

If n_- were so small that negligible current were carried by negative ions, there would be no need for a double layer. Second, the ratio of electron to negative-ion density must be larger in the sheath than in the plasma,

$$\left[\frac{n_e}{n_-}\right]_{\text{sheath}} > \left[\frac{n_e}{n_-}\right]_{\text{plasma}} \ . \tag{3}$$

Unless there is a change in average energy from one region to another, the double layer will not form; in an electronegative discharge, the difference in energy is manifested by a difference in the electron to negative-ion density ratio. This difference is maintained by a combination of field-dependent formation and loss rates and the disparity in ion and electron diffusivity and mobility.

Changes in power density affect the sheath dynamics in a manner which is consistent with the explanations offered above. The double layer takes less time to form at higher power and does not persist (within the sensitivity limits of the experiment) throughout the anodic half cycle [compare Figs. 5(a) and 5(b) or Figs. 2(b) and 2(c)]. The shorter formation time is consistent with faster extraction of the negative ions in the larger field at higher power. The fact that the double layer does not persist for as long suggests that the negative-ion density (relative to the electron density) is smaller at higher power [see Eq. (2)]; this could be caused by an increase in average electron energy and consequently a decrease in the attachment rate.

At higher frequencies, double-layer formation should be more difficult. Above ω_i, n_- is smaller because the EEDF has less time to cool as the applied field crosses zero and k_a will not show low-field enhancement. This prediction is verified below (also see Ref. 58).

2. *Sheath thickness*

As observed previously,[32] the sheath contracts when an electronegative gas is added to an electropositive discharge [Figs. 2(a) and 2(b)]. Although sheath contraction has been attributed to the difference in mobility between electrons and negative ions, Duke[69] has shown recently that differences in ionization potential may be more important. Sheath thickness scales with Debye length,[6,70]

$$\lambda_D = \left[\frac{\epsilon_0 T_e}{n e^2}\right]^{1/2} , \tag{4}$$

where ϵ_0 is the permittivity of free space, e is the electron charge, T_e is the electron temperature in the plasma (in volts), and n is the charge density in the plasma. Because Ar is not an attaching gas, n_- should decrease as BCl_3 is diluted; this effect is equivalent to an increase in T_e and, as observed, the sheath expands. T_e should increase also because Ar lacks the low-energy, inelastic collisional pathways (e.g., rotational and vibrational excitation) by which the EEDF is cooled in molecular gases such as BCl_3.

However, n also decreases as BCl_3 is diluted because the ionization potentials of B, Cl, and BCl_3 (8.3, 13, and 11.6 eV, respectively) are lower than the ionization potential for ground-state Ar (15.8 eV),[71] and more electrons have enough energy to ionize neutral species. From Eq. (4), a decrease in n results in a larger Debye length and, there-

fore, a larger sheath thickness. For $\leq$ 5 at. % HCl in He and Ar,[69] recent calculations suggest that the change in n and not T_e is dominant in determining the change in sheath thickness. Note that an increase in power density, which results mostly from an increase in current density and hence n (Fig. 1), results in a similar sheath contraction [Figs. 2(b) and 2(c)].

C. Effect of frequency on electronegative sheath dynamics

The frequency of the applied electric field plays an important role in determining the properties of both the plasma and the sheath. Above ω_i ($\sim$3 MHz), ions respond only to the time-averaged sheath field and displacement current exceeds ion conduction current in the sheath.[9,42–44,49,72] Below ω_i, ions respond to the instantaneous field and ion conduction current exceeds displacement current in the sheath. In both regimes, electron conduction current is dominant in the plasma unless, as we have seen above, Eq. (2) is satisfied.[58,73] Because the current is capacitively shunted across the sheath above ω_i (note the increased phase shift between current and voltage in Fig. 1), the instantaneous sheath fields are smaller for constant power.[43,49] This reduction in the sheath field magnitude is clearly evident in Figs. 2(d) and 7, where sheath fields are displayed as a color contour plot and as spatial profiles for ten different times during a 10-MHz rf cycle, respectively. The reduction in the sheath field magnitude is significant, although it is important to note that the accuracy and precision with which the fields are known at 10 MHz are less than for lower-frequency fields.[74] Besides the change in field magnitude, several other differences between high- and low-frequency sheaths are evident.

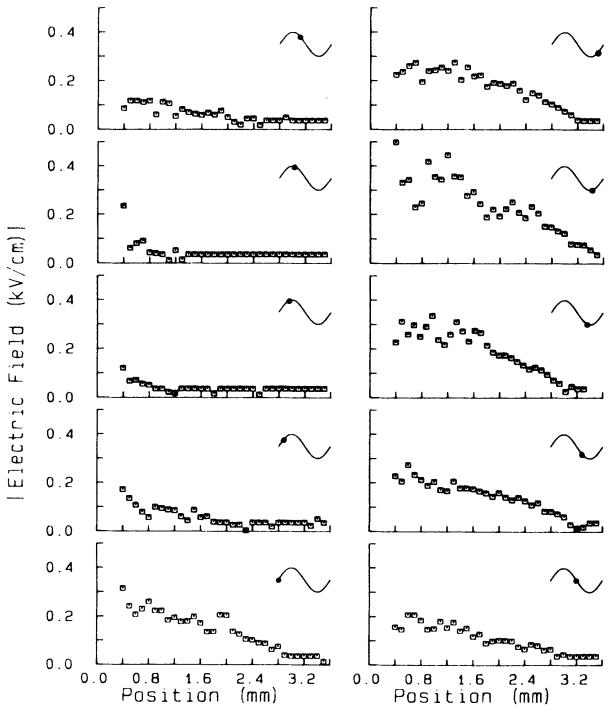

FIG. 7. Electric field magnitude vs position for ten different times during a 10-MHz rf cycle. The times at which the field is measured are shown in the diagrams to the right. These data are used in constructing the space-time contour plot of Fig. 2(d). See caption to Fig. 2(d) for discharge conditions.

1. Double layers

Double layers are not evident in pure BCl_3 discharges at high frequency. Thus, if the interpretation above is correct, either Eq. (2) or (3) must be violated. At higher frequencies, n_- is expected to be smaller because of incomplete relaxation of the low-energy part of the EEDF. Although several recent papers suggest that electron-energy relaxation is still fast compared to 10 MHz, this conclusion is based on temporally resolved optical emission measurements that sample only the high-energy tail of the EEDF.[20,42,75,76] Attachment rate enhancement observed at low frequency, however, relies on relaxation of the low-energy part of the EEDF. Depending on the gas and availability of low-energy inelastic pathways (e.g., vibrational and rotational excitation), the low-energy part of the EEDF may relax at a slower rate than the high-energy tail.[77,78] Recent calculations show that in molecular gases, the low-energy part of the EEDF does not relax as extensively as the high-energy part of the EEDF at 10 MHz.[77,79] As a result, k_a and n_- are smaller at higher frequency[58] and double layers are not evident.[80]

2. Sheath thickness

The increase in maximum sheath thickness from 2.4 mm at 50 kHz to 3.2 mm at 10 MHz seems surprising at first since the charge density is higher above ω_i (Refs. 39, 42, and 43) [see Eq. (4)]. Apparently this increase in n is more than compensated for by a decrease in the effective value of T_e, resulting from a larger n_- below ω_i. In an electropositive discharge, assuming that other factors such as secondary electron emission do not play a role, the sheath is expected to shrink as the frequency is increased from below to above ω_i because the charge density increases.

3. Sheath motion

As seen in Figs. 2(d) and 7, the sheath-plasma boundary oscillates above ω_i. This oscillation results from the electron response to the rf field and is the mechanism by which displacement current couples to conduction current in the plasma.[52] Because n_e in the sheath is modulated at 10 MHz, the net space charge density is also modulated and the sheath fields breath and impart energy to electrons. In agreement with theory,[8,52] the sheath oscillations are nearly symmetrical at high frequency compared to those at low frequency (Fig. 2). Because ions respond only to the time-averaged field at high frequency, positive charge is not depleted during the first quarter of the cathodic half cycle, the fields are not flat (compare Figs. 3, 4, and 7), and the time-averaged ion density is larger.[38,44]

4. *dc versus rf*

Because the sheaths are resistive and current is limited by ion conduction for both dc and low-frequency discharges, the sheath fields are expected to be similar. From Fig. 8, it is seen that the anodic and cathodic dc fields are similar to those in a 50-kHz discharge at the same power (compare with the appropriate parts of the rf cycle shown in Figs. 3 and 5). In particular, the sheath widths are the same within experimental accuracy (2.5 mm in the dc plasma versus 2.4 mm in the 50-kHz system) and a double layer is observed at the plasma-sheath boundary. The shape of the cathode field is similar to that found in the 50-kHz discharge when the electrode is the momentary cathode (Figs. 3 and 8).

Persistence of the double layer in the dc discharge suggests that the mean electron energy in the dc discharge is less than the corresponding energy in the 10-MHz discharge, which does not exhibit double layers. A colder EEDF for the dc discharge is consistent with a stationary sheath-plasma boundary and smaller conduction currents: A stationary sheath front does not impart energy to electrons; the current is smaller because it is limited by ion conduction. Thus, k_a and the double layers are larger in the dc discharge.

It is important to note that although the dc and low-frequency discharges appear similar for two times in the rf cycle, the effects of electron-energy modulation, attachment rate enhancement, detachment rate enhancement, and sheath motion have no dc analog. These effects certainly alter the energy distributions of particles in the plasma and particles impacting surfaces. As a result, the chemistry of the low-frequency rf discharge should differ from that of the dc discharge.

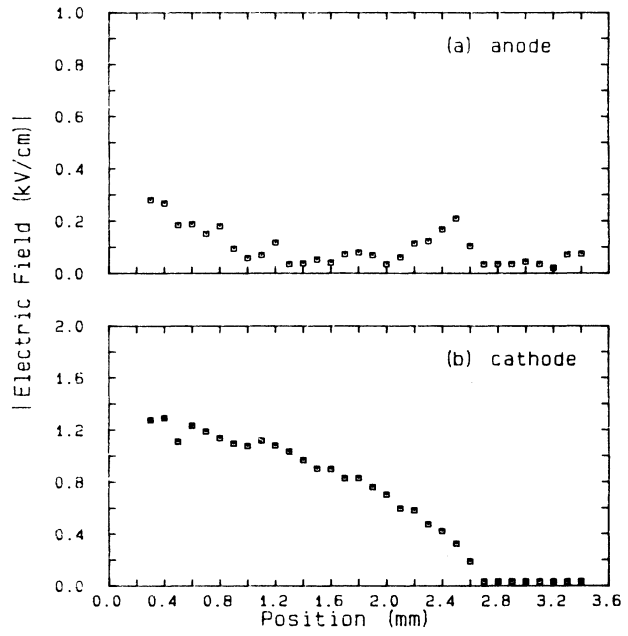

FIG. 8. Electric field magnitude vs position in (a) the cathode and (b) the anode sheath for a 10-W, dc discharge through nominally pure BCl_3 (see Ref. 56). Discharge conditions are same as for Fig. 2(a) except voltage $=360$ V, current $=0.028$ A, and power density $=0.14$ W cm^{-3}.

IV. SUMMARY

Thickness, shape, and motion of the sheath electric field in glow discharges containing BCl_3 are measured *in situ* and nonintrusively as a function of feedstock composition, power, and frequency. The space-time field maps presented here should be useful for testing self-consistent theories of rf discharges and for simulation studies of charged-particle transport to surfaces in contact with the plasma. Work along these lines is continuing.

Sheath thickness measurements provide information on charge density and average electron energy. For example, the sheath expands as BCl_3 is diluted with Ar because the charge density decreases and the average electron energy increases. The sheath also expands when the frequency is increased from 0.05 to 10 MHz because of a decrease in the negative-ion density which is equivalent to an increase in electron energy.

The shape of the electric field provides information about spatial variations in densities and rates. For example, the flat shape of the low-frequency field shows that charge is swept from the sheath as fast as it is formed. The negative slope of the high-frequency field shows that positive charge remains in the sheath because ion inertia limits the extraction rate. Field maxima at the plasma-sheath boundary indicate the presence of charge double layers, which result from spatially inhomogeneous attachment and detachment rates and the disparity between electron and ion diffusivity and mobility. Treating negative ions like cold electrons, this negative-ion double layer is analogous to the double layer found in a constricted positive column.

Motion of the plasma-sheath boundary provides information on charged-particle dynamics. At both low and high frequency, the sheath-plasma boundary oscillates. At low frequency, the large instantaneous fields sweep charge from the sheath so that the applied field penetrates further into the plasma and extracts additional charge. In this manner, ion conduction current couples to electron conduction current. At high frequency, ion inertia prevents an instantaneous response to the time-varying field and constrains the electrons to oscillate about the mean sheath-plasma boundary position. In this manner, sheath displacement current couples to electron conduction current.

During the time that this manuscript was originally submitted and subsequently revised, I received an unpublished report from J.-P. Boeuf (Ref. 68) describing a fluid model for electronegative and electropositive discharges over the frequency range considered in this paper. This model impressively reproduces most of the observations noted here.

ACKNOWLEDGMENTS

I am grateful to C. E. Gaebe, T. R. Hayes, M. L. Mandich, L. C. Pitchford, Y. M. Li, V. M. Donnelly, and R. S. Freund for stimulating conversations during the course of this work. The suggestion by T. Graedel to use color contour plots is deeply appreciated. I am also indebted to V. Godyak, L. C. Pitchford, Y. M. Li, and J.-P. Boeuf for sharing their results with me prior to publication.

[1]T. M. Mayer and R. A. Barker, J. Vac. Sci. Technol. **21**, 757 (1982).
[2]U. Gerlach-Meyer, J. W. Coburn, and E. Kay, Surf. Sci. **103**, 177 (1981).
[3]J. W. Coburn and E. Kay, J. Appl. Phys. **43**, 4965 (1972).
[4]B. Chapman, *Glow Discharge Processes* (Wiley, New York, 1980).
[5]N. Hershkowitz, Space Sci. Rev. **41**, 351 (1985).
[6]R. N. Franklin, *Plasma Phenomena in Gas Discharges* (Clarendon, Oxford, 1976).
[7]J. S. Levine and F. W. Crawford, J. Plasma Phys. **23**, 223 (1979).
[8]V. A. Godyak, *Soviet Radio Frequency Discharge Research* (Delphic Associates, Inc., Falls Church, VA, 1986).
[9]D. B. Graves and K. F. Jensen, IEEE Trans. Plasma Sci. **14**, 78 (1986).
[10]J. J. Lowke and D. K. Davies, J. Appl. Phys. **48**, 4991 (1977).
[11]B. Warner, Ph. D. thesis, University of Colorado, 1979.
[12]J. P. Boeuf, E. Marode, P. Segur, A. J. Davies, and J. G. Evans, in Proceedings of the Sixth International Conference on Gas Discharges, Edinburgh [IEE Conf. Publ. **189**, 63 (1980)].
[13]P. Segur, M. Yousfi, and E. Marode, in Proceedings of the Sixth International Conference on Gas Discharges, Edinburgh [IEE Conf. Publ. **189**, 56 (1980)].
[14]D. B. Graves, Bull. Am. Phys. Soc. **32**, 1167 (1986).
[15]A. D. Richards, B. E. Thompson, and H. H. Sawin, Appl. Phys. Lett. **50**, 492 (1987).
[16]M. J. Kushner, J. Appl. Phys. **54**, 4958 (1983).
[17]J. P. Boeuf and E. Marode, J. Phys. D **15**, 2169 (1982).
[18]Tran Ngoc An, E. Marode, and P. C. Johnson, J. Phys. D **10**, 2317 (1977).
[19]T. J. Moratz, L. C. Pitchford, and J. N. Bardsley, J. Appl. Phys. **61**, 2146 (1987).
[20]D. L. Flamm and V. M. Donnelly, Plasma Chem. Plasma. Proc. **1**, 317 (1981).
[21]J. W. Coburn, Plasma Chem. Plasma Proc. **2**, 1 (1982).
[22]D. W. Hess, Solid State Technol. **24**, 189 (1981).
[23]D. W. Hess, Plasma Chem. Plasma, Proc. **2**, 141 (1982).
[24]L. A. D'Asaro, A. D. Butherus, J. V. Dilorenzo, D. E. Iglesias, and S. H. Wemple, *Proceedings of the International Symposium on GaAs and Related Compounds, Vienna, 1980,* edited by H. W. Thim (IOP, London, 1981), p. 267.
[25]C. A. Moore, G. P. Davis, and R. A. Gottscho, Phys. Rev. Lett. **52**, 538 (1984).
[26]M. L. Mandich, C. E. Gaebe, and R. A. Gottscho, J. Chem. Phys. **83**, 3349 (1985).
[27]D. K. Doughty and J. E. Lawler, Appl. Phys. Lett. **45**, 611 (1984).
[28]B. N. Ganguly and A. Garscadden, Appl. Phys. Lett. **46**, 540 (1985).
[29]B. N. Ganguly and A. Garscadden, Phys. Rev. A **32**, 2544 (1985).
[30]B. N. Ganguly, J. Appl. Phys. **60**, 571 (1986).
[31]J. Derouard and N. Sadeghi, Opt. Commun. **57**, 239 (1986).
[32]K. G. Emeleus and G. A. Woolsey, *Discharges in Electronegative Gases* (Barnes and Noble, New York, 1970).
[33]H. S. W. Massey, *Negative Ions* (Cambridge University Press, Cambridge, 1976).
[34]J. B. Thompson, Proc. Phys. Soc. **73**, 818 (1959).
[35]K. G. Emeleus, Int. J. Electron. **61**, 281 (1986).
[36]A. Garscadden, in *Gaseous Electronics,* edited by N. Hirsh and H. Oskam (Academic, New York, 1978), Vol. 1.
[37]G. L. Rogoff, J. Phys. D **18**, 1533 (1985).
[38]V. M. Donnelly, D. L. Flamm, and G. Collins, J. Vac. Sci. Technol. **21**, 817 (1982).
[39]D. E. Ibbotson, D. L. Flamm, and V. M. Donnelly, J. Appl. Phys. **54**, 5974 (1983).
[40]D. L. Flamm and V. M. Donnelly, J. Appl. Phys. **59**, 1052 (1986).
[41]V. M. Donnelly, D. L. Flamm, and R. H. Bruce, J. Appl. Phys. **58**, 2135 (1985).
[42]D. L. Flamm, J. Vac. Sci. Technol. A **4**, 729 (1986).
[43]R. A. Gottscho and M. L. Mandich, J. Vac. Sci. Technol. A **3**, 617 (1985).
[44]R. H. Bruce, J. Appl. Phys. **52**, 7064 (1981).
[45]C. M. Ferreira and J. Loureiro, J. Phys. D **17**, 1175 (1984).
[46]R. Claude, M. Moisan, and M. R. Wertheimer, in Plasma Processing, edited by J. W. Coburn, R. A. Gottscho, and D. W. Hess [Mat. Res. Soc. Symp. Proc. **68**, 85 (1986)].
[47]R. H. Bruce, Solid State Technol. **24**, 64 (1981).
[48]C. B. Zarowin, J. Electrochem. Soc. **130**, 1144 (1983).
[49]C. B. Zarowin, J. Vac. Sci. Technol. A **2**, 1537 (1984).
[50]P. Briaud, G. Turban, and B. Grolleau, in Plasma Processing, edited by J. W. Coburn, R. A. Gottscho, and D. W. Hess [Mater. Res. Soc. Symp. **68**, 109 (1986)].
[51]R. W. Gould, Phys. Lett. **11**, 236 (1964).
[52]V. A. Godyak, Fiz. Plazmy **2**, 141 (1976) [Sov. J. Plasma Phys. **2**, 78 (1976)].
[53]O. A. Popov and V. A. Godyak, J. Appl. Phys. **57**, 53 (1985).
[54]R. A. Gottscho, R. H. Burton, D. L. Flamm, V. M. Donnelly, and G. P. Davis, J. Appl. Phys. **55**, 2707 (1984).
[55]Although Matheson's stated purity is $>99.7\%$, Reents (Ref. 56) has shown that the purity is typically 86.2% with the major impurities being $BFCl_2$ (8.3%), BF_3 (3.8%), BF_2Cl (0.71%), and HCl (0.68%). The HCl concentration varies by as much as ten times depending on the gas bottle age, how the gas is extracted, and flow rate.
[56]W. D. Reents (unpublished).
[57]R. A. Gottscho, G. P. Davis, and R. H. Burton, Plasma Chem. Plasma Proc. **3**, 193 (1983); J. Vac. Sci. Technol. A **1**, 622 (1983).
[58]R. A. Gottscho and C. E. Gaebe, IEEE Trans. Plasma Sci. **14**, 92 (1986).
[59]R. K. Smith, W. P. Petersen, and J. A. O'Sullivan (unpublished results).
[60]T. E. Gradedel and R. McGill, Science **215**, 1191 (1982).
[61]A. L. Cappelli, R. A. Gottscho, and T. A. Miller, Plasma Chem. Plasma Proc. **5**, 317 (1985).
[62]R. A. Gottscho and V. M. Donnelly, J. Appl. Phys. **56**, 245

(1984).
[63]D. A. Scott and A. V. Phelps, Bull. Am. Phys. Soc. **32**, 1158 (1987).
[64]A. S. Kovalev, A. T. Rakhimov, and V. A. Feoktistov, Fiz. Plazmy **8**, 1093 (1982) [Sov. J. Plasma Phys. **8**, 622 (1982)].
[65]A. D. Barkalov and G. G. Gladush, Zh. Tekhn. Fiz. **49**, 2183 (1979) [Sov. Phys.—Tech. Phys. **24**, 1203 (1979)].
[66]J. A. Stockdale, D. R. Nelson, F. J. Davis, and R. N. Compton, J. Chem. Phys. **56**, 3336 (1972).
[67]M. S. Huq, D. Scott, N. R. White, R. L. Champion, and L. D. Doverspike, J. Chem. Phys. **80**, 3651 (1984).
[68]J.-P. Boeuf, Phys. Rev. A (to be published).
[69]G. L. Duke, Bull. Am. Phys. Soc. **29**, 150 (1984); Ph. D. thesis, Air Force Institute of Technology, Report No. AFWAL-TR-84-2099, 1985 (unpublished).
[70]V. E. Golant, A. P. Zhilinsky, and I. E. Sakharov, *Fundamentals of Plasma Physics* (Wiley, New York, 1977), p. 12.
[71]H. M. Rosenstock, K. Draxl, B. W. Steiner, and J. T. Herron, J. Phys. Chem. Ref. Data **6**, Suppl. 1 (1977).
[72]W. C. Dautremont-Smith, R. A. Gottscho, and R. J. Schutz, in *Semiconductor Materials and Process Technologies,* edited by G. E. McGuire (Noyes, Park Ridge, N.J., in press), p. 191.
[73]G. L. Rogoff, J. M. Kramer, and R. B. Piejak, IEEE Trans. Plasma Sci. **14**, 103 (1986).
[74]The uncertainty in these measurements is greater than those obtained at lower frequencies for two reasons. First, a 10-ns gate is used in recording the Stark-mixed fluorescence intensities at high frequency as opposed to the 20-ns gate used at lower frequencies. Thus, the signal collected is smaller. In addition, the fields may still very significantly during the time the gate is opened and the measured intensity ratio is a nonlinear average over this gate duration. We estimate the error resulting from this finite time resolution to be no more than 50 V/cm, assuming that the field varies sinusoidally. This error is systematic, however, so that measurements made while the field is decreasing can be 50 V/cm low, while those made while the field is increasing can be 50 V/cm high. The finite time resolution can affect the shape of the spatial profiles only if the time dependence of the field is different for different positions. A second source of error in the measurements at 10 MHz stems from uncertainties in the calibration curve used to invert the raw line intensity ratios to absolute field values. In Ref. 26 calibration curves of the form $Q/R = \alpha E^2/(1+\beta E^2)+C$, where Q/R is the line intensity ratio, E is the electric field, and α, β, and C are empirical fitting parameters, were used to invert line intensity ratios to electric field magnitudes. For the 10-ns gate width, we determined preliminary calibration constants for the $P(6)$ rotational line at 0.3 Torr to be $\alpha = 9.620 \times 10^{-6}$, $\beta = 1.393 \times 10^{-5}$, and $C = 0.0095$. Because of the uncertainty in these calibration constants, the precision with which field measurements are made at 10 MHz with a 10-ns gate is believed to be not better than $\pm$ 50 V/cm and the detection limit to be no better than 100 V/cm. A measure of the precision and accuracy of the field measurements is obtained by comparing the total voltage drop across the sheaths to that measured across the gap with a high voltage probe. For the 10-MHz discharge at 10 W, the measured peak voltage is 200$\pm$20 V; the integrated field measurements account for only half of this voltage, assuming that the plasma potential.
[75]G. Rosny, E. R. Mosburg, Jr., J. R. Abelson, G. Devaud, and R. C. Kerns, J. Appl. Phys. **54**, 2272 (1983).
[76]P. Bletzinger and C. A. DeJoseph, Jr., IEEE Trans. Plasma Sci. **14**, 124 (1986).
[77]Y. Li and L. C. Pitchford (unpublished results).
[78]M. Dilonardo, M. Capitelli, R. Winkler, and J. Wilhelm, in Plasma Processing, edited by J. W. Coburn, R. A. Gottscho, and D. W. Hess [Mater. Res. Soc. Sym. Proc. **68**, 287 (1986)].
[79]L. Kline (private communication).
[80]It is important to keep in mind that the sensitivity with which field magnitudes are measured is 75 V/cm. Any conclusions about the absence of double layers only apply to features whose magnitude are larger than this limit. It is the author's belief that more sensitive field measurements are likely to uncover small double layers in the higher-frequency discharges.

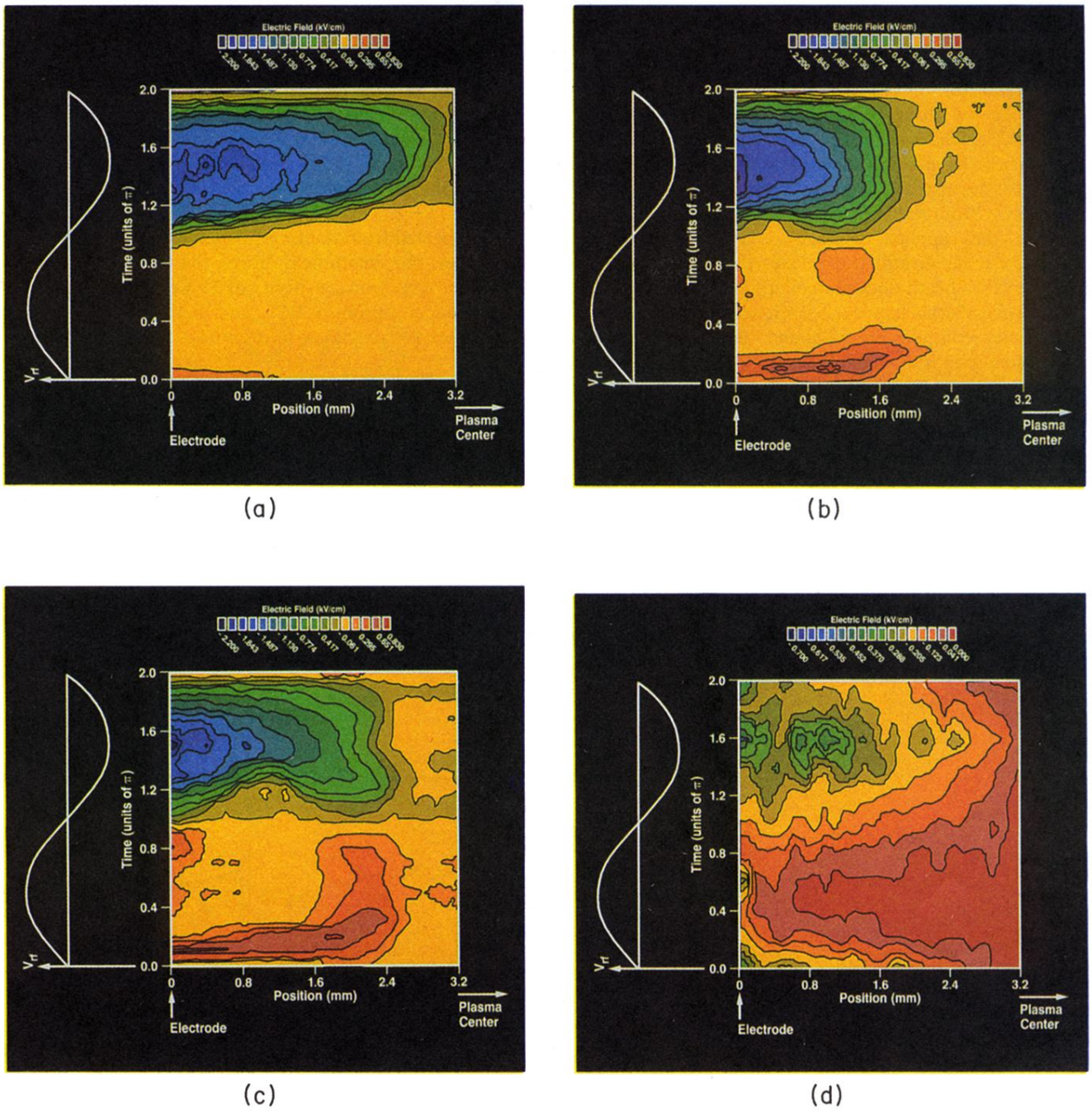

FIG. 2. (a) Color contour plot of sheath electric fields in 50-kHz discharge through 95 at. % Ar and 5 at. % BCl_3. The position of the electrode is at 0 mm and the plasma center (not shown) is at 8.0 mm. Time in units of π refers to the phase of the applied voltage on the electrode at 0 mm as shown by the sine wave on the left. The color scale is shown at the top; the sign of the field is assumed to be positive from $\omega t = 0$ to π and negative from $\omega t = \pi$ to 2π. The plot is generated by linearly interpolating measurements made at 20 equally spaced times during the rf cycle and 32 equally spaced positions in the sheath to a 100×100 space-time array. References 59 and 60 contain additional details on the generation of such plots. Discharge conditions are (see text for measurement precision and accuracy): total flow rate 10 sccm, Ar flow rate 9.5 sccm, BCl_3 flow rate 0.5 sccm, rms voltage 508 V, peak voltage 711 V, rms current 0.064 A, peak current 0.090 A, power 30 W, power density 0.41 W cm^{-3}, pressure 0.3 Torr. (b) Same as (a) except for nominally pure BCl_3 (see Ref. 56). Discharge conditions are the same as for (a) except rms voltage is 354 V, peak voltage is 476 V, rms current is 0.090 A, peak current is 0.146 A. (c) Same as (a) except for nominally pure BCl_3 (see Ref. 56) 10-W, 50-kHz discharge. The sign of the electric field was determined from photodetachment optogalvanic measurements (see Ref. 58). Discharge conditions are the same as for (a) except rms voltage is 274 V, peak voltage is 380 V, rms current is 0.038 A, peak current is 0.065 A, and power density is 0.14 W cm^{-3}. (d) Same as (a) except for nominally pure BCl_3 (see Ref. 56) 10-W, 10-MHz discharge. Discharge conditions are same as for (a) except rms voltage is 147 V, peak voltage is 204 V, rms current is 0.191 A, peak current is 0.281 A, and power density is 0.14 W cm^{-3}. Here, the 100×100 interpolated array is constructed from measurements made at 10 equally spaced times in the rf cycle and 32 equally spaced positions in the rf sheath.